Understanding Noncovalent Interactions of Small Molecules with Carbon Nanotubes

Joaquín Calbo, Alejandro López-Moreno, Alberto de Juan, Jeffrey Comer, Enrique Ortí, Emilio M. Pérez

Understanding Noncovalent Interactions of Small Molecules with Carbon Nanotubes

Joaquín Calbo,[a] Alejandro López-Moreno,[b] Alberto de Juan,[b] Jeffrey Comer,[c*] Enrique Ortí,[a,*] Emilio M. Pérez[b,*]

Abstract: We combine experiment, density functional theory (DFT) and molecular dynamics (MD) simulations for the quantitative analyses of the noncovalent interaction between (6,5)-enriched single-walled carbon nanotubes (SWNTs), as hosts, and a set of pyrene derivatives with different electronic properties and surface area, as guests. The experiments and calculations were carried out in two solvents with markedly different polarities: 1,1',2,2'-tetrachloroethane (TCE) and N,N-dimethylformamide (DMF). Our results show that dispersion forces govern the supramolecular association of small molecules with (6,5)-SWNTs, with negligible contribution from ground-state charge-transfer effects. In the nonpolar solvent (TCE), the binding constant is highly correlated with the contact area between the SWNT and the guests. In the polar solvent (DMF), binding constant has a complex dependence on the chemical nature of the pyrene substituents, as demonstrated by MD simulations with explicit inclusion of solvent molecules. Solvation of the small-molecules is shown to play a leading role in the binding process. Remarkably, the binding constants obtained from MD simulation over the five guest molecules are correlated with those derived from experiment. Furthermore, the MD simulations also reveal the structure of adsorbed guest from low to high SWNT surface coverage.

Introduction

The supramolecular chemistry of carbon nanotubes was kick-started by Dai's[1] and Nakashima's[2] reports on the decoration of their sidewalls with pyrene derivatives. The Stanford group used pyrene as a noncovalent anchor to attach biomolecules, while the Japanese group used ammonium salts covalently attached to pyrene to help solubilize the carbon material in water. Since these seminal contributions, the noncovalent chemistry of carbon nanotubes has been particularly fruitful.[3-6] For example, Guldi and Prato et al. reported pyrene- and porphyrin-based single-walled carbon nanotube (SWNT) assemblies leading to novel electron donor-acceptor nanohybrids, which upon photoexcitation undergo fast electron transfer followed by the generation of microsecond-lived charge-separated species.[7-9] On the other hand, the generation of noncovalent SWNT hybrids has promoted the fabrication of SWNT/field-effect transistor (FET) devices with appealing conductivity and tunable photosensitization properties.[10-12] Oligo- or polymeric structures have also been used, and have been particularly successful at addressing the sorting of SWNTs according to their diameter/chirality.[13-22] Importantly, DNA has been shown to bind to SWNTs in a sequence-specific manner, which was exploited for the purification of SWNTs according to their chirality.[23]

Despite all these success stories, the overwhelming majority of reports on noncovalent derivatives of SWNTs are based exclusively on qualitative experimental observations.[3-4, 6] In contrast to soluble host-guest systems, in which the accurate determination of association constants constitutes the basis for any further discussion, the heterogeneous structure of the SWNTs and their characteristic insolubility hinder the determination of the molar concentration of SWNTs in solution, which prevents a deep understanding of the factors governing the supramolecular association of SWNTs. Needless to say, the lack of quantitative and comparable information represents a major obstacle in the progress of the supramolecular chemistry of SWNTs.

Several attempts at tackling this problem have already been made. From the experimental point of view, skillfully designed atomic force microscopy experiments have allowed for the measurement of interaction forces between molecules and SWNTs. For instance, single-molecule force spectroscopy has been used to measure the force required to remove single-stranded DNA homopolymers from SWNTs.[24] On the other hand, a kinetic model for quantification of chirality-specific interactions of SWNTs with hydrogels has also been reported,[25] providing foundation for both the mechanistic understanding of gel-based SWNT separation as well as the potential industrial-scale realization of single-chirality production of carbon nanotubes. Finally, a new and simple procedure for the quantitative determination of association constants between soluble molecules and insoluble carbon nanotube samples has been recently presented by some of us, and applied to a series of pyrene-based guests of increasing size for the first time.[26] Particularly interesting is the fact that this protocol was sensitive to solvent effects as well as small structural changes in both the guest (chemical substitution) and host (nanotube diameter) systems.

In silico investigations on SWNT-based supramolecular chemistry are far more abundant, and a wide variety of DFT methods have already been tested.[27] Dispersion-accounting

[a] Dr. J. Calbo, Prof. E. Ortí
Instituto de Ciencia Molecular, Universidad de Valencia,
46980 Paterna, Spain
Email: enrique.orti@uv.es
[b] Dr. A. López-Moreno, Dr. A. de Juan, Prof. E.M. Pérez
IMDEA Nanociencia, Ciudad Universitaria de Cantoblanco,
28049 Madrid, Spain
Email: emilio.perez@imdea.org
[c] Dr. J. Comer
Department of Anatomy and Physiology, Kansas State University,
Manhattan, Kansas, 66506
Email: jeffcomer@ksu.edu

Supporting information for this article is given via a link at the end of the document.

DFT approaches stand as accurate yet affordable methodologies giving quantitative predictions on noncovalent interactions with chemical accuracy.[28-30] Among them, the Grimme's dispersion-correction (so called D3) is the most popular *ab initio* approach to deal with the weak noncovalent interactions where the 'gold-standard' coupled-cluster CCSD(T) becomes prohibitive.[31-32]

Although a significant effort from the theoretical community has helped to partially compensate for the lack of quantitative experimental data, *in silico* experiments are usually performed in the gas phase, where solvophobic interactions are not considered. Alternatively, classical molecular dynamics simulations with atomistic models and explicit solvent have arisen as a promising approach to elucidate interactions between common nanomaterials and organic molecules. Free-energy techniques have been used to calculate adsorption affinities of amino acids on model gold,[33-36] silver,[37] zinc oxide surfaces,[38] and graphenic materials,[39-40] as well as for contaminants on amorphous silica.[41] Likewise, Ulissi et al.[42] reported free energies of adsorption on a graphenic surface for more than 50 compounds, showing a good correlation with the predictions of structure–activity models. Finally, coauthors of the present work have recently reported a molecular dynamics protocol capable of predicting adsorption affinities of small aromatic molecules on carbon nanotubes with excellent correlation ($R^2 \geq 0.83$) between calculated and measured values of the logarithm of the adsorption equilibrium constant.[43]

In this work, we report on an in-depth investigation on the supramolecular assembly of small-molecule derivatives with insoluble carbon-based nanotubes governed by noncovalent interactions through a combined experimental–computational quantitative approach. The association constant (K_a) of a series of pyrene-based guests with SWNT is attained experimentally by means of a quantitative thermogravimetric protocol. The effect of the guest electronic character and of the solvent polarity are revealed along the series of electron-donor and electron-acceptor pyrene derivatives as well as with the use of DMF and TCE as solvents. State-of-the-art calculations at the dispersion-corrected DFT-D3 level are employed to quantify the interaction between the different pyrene-based derivatives with SWNT, both in gas phase and using continuum solvent effects, whereas molecular dynamics with explicit solvent molecules were performed to fully understand the supramolecular recognition events in solution. Disentangling and quantifying the subtle effects originating the noncovalent host-guest recognition of SWNTs by small aromatic molecules will undoubtedly help advance the supramolecular chemistry of carbon nanotubes and carbon-based nanomaterials.

Results and Discussion

Experimental association constants: We started by measuring the binding constants of a series of pyrene-based guests with SWNTs by performing titration experiments as described previously.[26] Briefly, to solutions of different concentration of guest, 1 mg/mL of SWNTs was added and stirred for 2 hours. Then, the suspension was filtered through polytetrafluorethylene (PTFE) membrane of 0.2 µm of pore size and dried under vacuum. Thermogravimetric analysis (TGA) of the solid obtained was carried out in nitrogen, to quantify the amount of guest molecule adsorbed. We used a collection of pyrene derivatives showing different electronic character, from electron-acceptor to electron-donor molecules. Titrations vs (6,5)-enriched SWNTs were carried out with pyrene (**1**), 1,6-pyrendione (**2**), 1,8-pyrenedione (**3**), 1,6-diaminopyrene (**4**) and 2,7-dimethoxypyrene (**5**) obtaining the binding isotherms showed in Figure 1 and the binding constants summarized in Table 1. All experiments cover at least 70% of the binding isotherm. The titration experiments carried out in DMF afforded log $K_a = 0.20 \pm 0.11$ M^{-1}, 2.08 ± 0.04 M^{-1}, 1.76 ± 0.04 M^{-1}, 1.43 ± 0.05 M^{-1} and 1.73 ± 0.08 M^{-1} for guests **1**, **2**, **3**, **4**, and **5**, respectively. While in TCE guest **1** showed an identical constant, log $K_a = 0.20 \pm 0.03$ M^{-1}, the rest of guests present significant differences between solvents, with log $K_a = 3.20 \pm 0.14$ M^{-1}, 2.04 ± 0.08 M^{-1}, 2.84 ± 0.06 M^{-1} and 1.59 ± 0.14 M^{-1} for **2**, **3**, **4**, and **5**, respectively, in TCE.

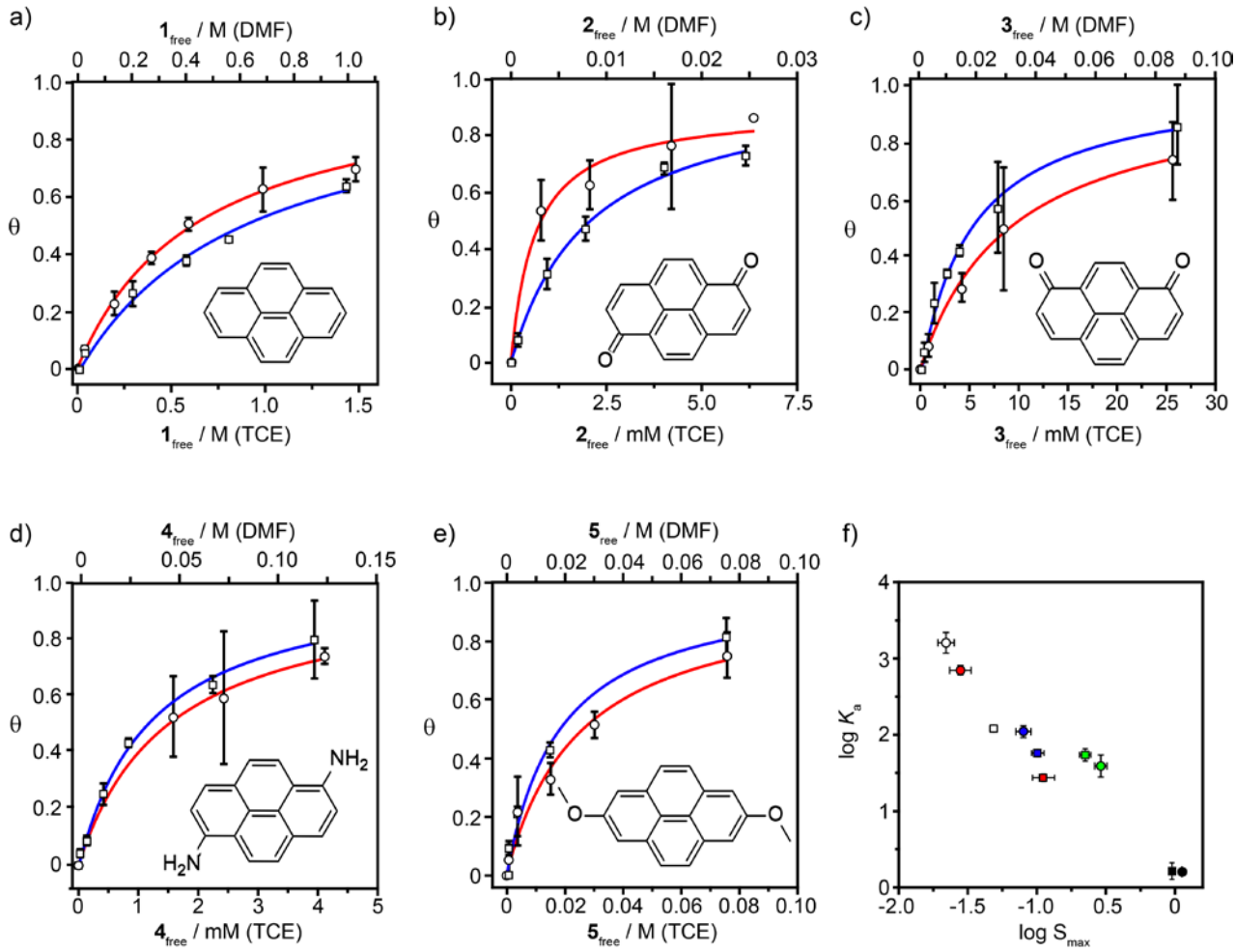

Figure 1. Titrations vs (6,5)-SWNTs (1 mg mL^{-1}) in DMF (blue curve) and TCE (red curve) of (a) pyrene (**1**), (b) 1,6-pyrenedione (**2**), (c) 1,8-pyrenedione (**3**), (d) 1,6-diaminopyrene (**4**), and (e) 2,7-dimethoxypyrene (**5**). (f) Logarithm of association constant vs logarithm of maximum solubility of guest molecules (1: black, 2: white, 3: blue, 4: red, and 5: green) in TCE (circles) and DMF (squares). Each data point is the average of three separate experiments, and the error bars represent the standard deviation .

Table 1. Results from titrations and solubility at 298 K. Errors are ± standard deviation.

Chemical Structure	Guest	Solvent	log K_a	R^2	log $S_{max.}$
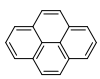	**1**	DMF	0.20 ± 0.11	0.987	−0.03 ± 0.01
		TCE	0.20 ± 0.03	0.998	0.05 ± 0.02
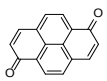	**2**	DMF	2.08 ± 0.04	0.997	−1.32 ± 0.03
		TCE	3.20 ± 0.14	0.977	−1.66 ± 0.03
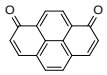	**3**	DMF	1.76 ± 0.04	0.993	−1.00 ± 0.04
		TCE	2.04 ± 0.08	0.994	−1.10 ± 0.05
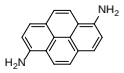	**4**	DMF	1.43 ± 0.05	0.996	−0.96 ± 0.08
		TCE	2.84 ± 0.06	0.996	−1.55 ± 0.08
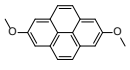	**5**	DMF	1.73 ± 0.08	0.991	−0.66 ± 0.04
		TCE	1.59 ± 0.14	0.967	−0.54 ± 0.04

The solubility at saturation of each molecule was calculated in both solvents to study the relationship between binding constant and solubility (S_{max}). Interestingly, a linear relationship between log K_a and log S_{max} is observed (Figure 1f). This fact shows that the contribution of the solvation enthalpy is predominant in this kind of supramolecular systems.

In order to study the contribution of the electronic character of the guest molecules to their association with SWNTs, an extensive characterization of host (SWNTs), guest (pyrene derivatives) and their supramolecular complexes was carried out in TCE and DMF.

First, to quantitatively evaluate the electronic properties of the guests, the electrochemical characterization of guests **1**–**5** was carried out in DMF using tetrabutylammonium perchlorate (TBAP) as electrolyte (Figure S1). The results are shown in Table 2. Reversible reduction waves at half-wave potentials were obtained for **1** ($E_{1/2}$ = –1.91 V), **2** ($E_{1/2}^1$ = –0.23 V and $E_{1/2}^2$ = –0.68 V), **3** ($E_{1/2}^1$ = –0.23 V and $E_{1/2}^2$ = –0.52 V), and **5** ($E_{1/2}$ =

–1.86 V), and two oxidation waves for **4** ($E_{1/2}^1$ = 0.37 V and $E_{1/2}^2$ = 0.62 V) with respect to Ag/AgCl. Pyrenedione derivatives **2** and **3** therefore exhibit low reduction potentials with corresponding low LUMO energy levels, confirming their electron-acceptor behavior.[44] In contrast, the electron-donating character of the pyrenediamine derivative **4** is evidenced by the low oxidation potential recorded experimentally, in line with a high energy HOMO level in comparison with **2** and **3** (Table 2).

Table 2 Electrochemical data of molecules **1**–**5**, and experimentally determined HOMO and LUMO energy levels.

Molecule	$E_{1/2}^{red}$ (V)	E_{red}^{onset} (V)	E_g[a] (eV)	LUMO[b] (eV)	HOMO[b] (eV)
1	–1.91	–1.80	3.54	–2.60	–6.14
2	–0.23	–0.14	2.80	–4.26	–6.74
3	–0.23	–0.13	2.28	–4.27	–6.55
5	–1.86	–1.77	3.52	–2.63	–6.15
Molecule	$E_{1/2}^{ox}$ (V)	E_{ox}^{onset} (V)	E_g[a] (eV)	LUMO[b] (eV)	HOMO[b] (eV)
4	0.37	0.32	2.70	–2.02	–4.72

[a] The optical bandgap (E_g) was determined using the UV-vis spectra of the molecule and applying E_g = 1240/ λ_{abs} where λ_{abs} is the wavelength at which absorption starts.

[b] The LUMO energy was calculated using the follow equation: $E_{LUMO} = -E_{red}^{onset} - 4.4$ V and the HOMO energy by subtraction of E_g for compounds **1**, **2**, **3** and **5**. The HOMO energy was calculated using the follow equation: $E_{LUMO} = -E_{ox}^{onset} - 4.4$ V and the LUMO energy by addition of E_g for compound **4**.

Despite the different electronic character of guests **1**-**5**, the UV-vis-NIR spectra (Figure S2 and S3) reveal no shifts in their absorption band upon attachment to the sidewalls of the SWNTs. For **1** in DMF, the maximum of absorption is observed at 337 nm, which is not shifted in **1**•SWNTs. The same behavior is observed for **5** and **5**•SWNTs (340 nm). In the rest of complexes (**2**•SWNTs, **3**•SWNTs, and **4**•SWNTs) no clear absorption due to the molecule is observed, and only (6,5)-SWNTs absorption is noticeable. The trend is corroborated by comparison between the emission spectra of the free molecule and the emission of the molecule attached to the nanotube in both solvents (Figure S4 and S5). All spectra were normalized to compare them. In accordance with the absorption spectra, no shifts were observed between the photoluminescence spectra of the free guests and that of the complexes. Only slight changes in the band structure are observed for **4**•SWNTs and **5**•SWNTs with TCE as solvent. These results indicate that the typical optical features of the SWNT are preserved upon complexation with the pyrene-based derivatives.

The characterization by Raman spectroscopy is shown in Figure S6 and S7. The spectra (λ_{exc} = 785 nm) of pristine SWNTs and all the complexes are very similar, thus proving that the structure of the nanotubes is preserved in both solvents, with no increase in the relative intensity of the characteristic D-band. The G-band of samples from titrations in DMF is shifted from 1583 cm^{-1} ((6,5)-SWNT) to 1581 cm^{-1}, 1586 cm^{-1}, 1582 cm^{-1}, and 1580 cm^{-1} for **1**•SWNTs, **2**•SWNTs, **4**•SWNTs, and **5**·SWNTs, respectively, while no shift is observed for **3**•SWNTs. In TCE, similar shifts are observed in the G-band from 1588 cm^{-1} in the (6,5)-SWNTs to 1587 cm^{-1}, 1586 cm^{-1}, 1582 cm^{-1}, 1582 cm^{-1}, and 1586 cm^{-1} for **1**•SWNTs, **2**•SWNTs, **3**•SWNTs, **4**•SWNTs, and **5**•SWNTs, respectively. All these spectroscopic results suggest that there is no significant charge-transfer between the guests and the SWNTs in the ground state.

DFT Calculations: Theoretical calculations were performed for the list of host-guest nanotube-based assemblies by means of the density functional theory (DFT). Interaction energies as well as deformation barriers were calculated as described in the Methods Section. Figure 2 displays the minimum-energy geometries for the **1**–**5** guests assembled with the $C_{132}H_{22}$ model of (6,5)-SWNT computed at the PBE0-D3/6-31G** level of theory in gas phase (see the Supporting Information and Figure S8 for more details). Slight differences in how the guest is accommodated over the nanotube surface are predicted for **1**–**5** derivatives. Assemblies **1**•(6,5)-SWNT and **4**•(6,5)-SWNT present an almost parallel orientation of the longest pyrene molecular axis with respect to the nanotube growth direction (angle φ equal to 11.7 and 15.3º, respectively; see Figure 2). In contrast, complexes **2**•, **3**•, and **5**•(6,5)-SWNT show a more diagonal disposition with angle φ = 59.6, 67.7, and 39.8º, respectively. The π–π interactions between the host and the guest in the range of 3.2–3.7 Å stabilize the formation of the complex in all host-guest assemblies (Figure S9). The complex formed by the pristine pyrene is calculated with a moderate interaction energy (E_{int}) of –16.90 kcal/mol at the PBE0-D3/6-31G** level including counterpoise (CP) and three-body dispersion (E^{ABC}) corrections (see Methods for further details). Moving to the electron-acceptor pyrenedione guests **2** and **3**, the interaction energy when coupled to (6,5)-SWNT slightly increases in approximately 1 kcal/mol (Table 3). Otherwise, guest **4**, with amine groups, stabilizes the complex up to –21.34 kcal/mol due to the favorable close NH···nanotube contacts computed in the range of 2.8–3.2 Å (Figure S9). Finally, guest **5** is found to associate (6,5)-SWNT with similar interaction energy of –21.03 kcal/mol. In this system, not only π–π but also *n*(O)–π and CH–π interactions arise between the methoxy groups and the nanotube surface.

Since the pyrene-based guest system is inherently rigid, the deformation energy (E_{def}) upon formation of the supramolecular assembly is expected to be rather small. In fact, the E_{def} calculated for the series at the PBE0-D3/6-31G** level is in the range of 0.23−1.43 kcal/mol. Supramolecular assemblies containing guests with more diagonal dispositions (**3**•(6,5)-SWNT) and with more flexible substituent groups (**4**•(6,5)-SWNT and **5**•(6,5)-SWNT) show the largest deformation energies (Table 3). However, the global effect on the final binding energy (E_{bind}) is at most 8%. The trends found for E_{int} are therefore kept in the E_{bind} values ($E_{bind} = E_{int} + E_{def}$).

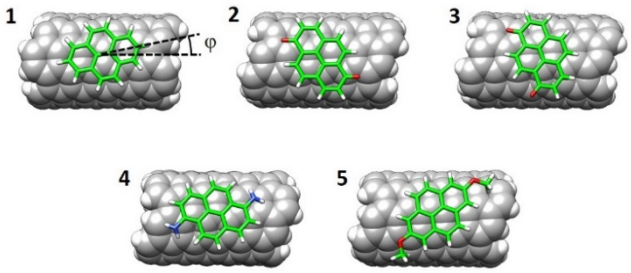

Figure 2. Minimum-energy geometries calculated for the supramolecular assemblies formed by guests **1**–**5** *vs* (6,5)-SWNT at the PBE0-D3/6-31G** level of theory. The definition of angle *φ* between the nanotube and the guest is indicated in **1**.

The electronic charge transfer in the ground state was quantified by summing the Mulliken atomic charges calculated for the nanotube and the pyrene-based guest at the PBE0-D3/6-31G** level in gas phase. Theoretical calculations predict negligible charge transfer in all the minimum-energy structures **1–5**•(6,5)-SWNT. Accumulated charges show a slight electron donation of 0.02e from the guest to the nanotube in systems **1**•(6,5)-SWNT and **4**•(6,5)-SWNT, whereas a negligible charge transfer of less than 0.01e is calculated for **5**•(6,5)-SWNT. Otherwise, a charge of only 0.01e is retrieved from the nanotube when assembled with the electron-acceptor guests **2** and **3**. Theoretical calculations including solvent effects provide equivalent results in terms of electronic charge transfer (Table S1). The negligible charge transfer predicted theoretically supports the marginal changes observed in the electronic and Raman spectra upon complex formation.

The origin of the stabilization in the supramolecular assemblies should therefore mainly come from the amount of noncovalent interactions. A parameter directly related with these interactions is the intermolecular contact area (ICA) between the host and the guest. The ICA was computed for the minimum-energy geometries of all the complexes (Table 3), and the relationship between the interaction energy E_{int} and the ICA is displayed in Figure 3. A good correlation is predicted for the stabilizing E_{int} with respect to ICA, in spite of the relatively small range of the total stabilizing interaction (< 4.5 kcal/mol). The main outlier is found for complex **4**•(6,5)-SWNT, for which the pyrene derivative containing amino groups provide short NH···SWNT discrete interactions (Figure S9), with the corresponding significant increase of the final interaction energy. These results clearly show that the stabilization of the supramolecular assembly is directly related to the number of close contacts between host and guest systems, in line with recent evidences reported for semiconducting copolymer-nanotube hybrids.[45]

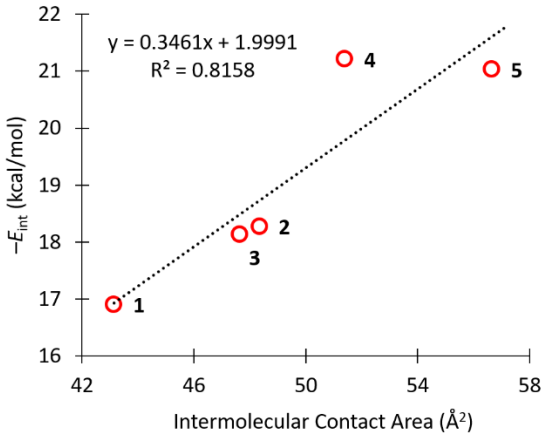

Figure 3. Relationship between the interaction energy and the intermolecular contact area for the **1–5**•(6,5)-SWNT assemblies.

Table 3 Energetic parameters (in kcal/mol) and intermolecular contact area (ICA, in Å²) computed for the interaction between guests 1–5 and host (6,5)-SWNT at the CP-corrected PBE0-D3/6-31G**+E^{ABC} level of theory.

Assembly	E_{int}	E_{def}	E_{bind}	ICA[a]
1·(6,5)-SWNT	–16.90	0.23	–16.67	43.15
2·(6,5)-SWNT	–18.27	0.41	–17.86	48.35
3·(6,5)-SWNT	–18.13	1.03	–16.82	47.65
4·(6,5)-SWNT	–21.34	0.72	–20.62	51.40
5·(6,5)-SWNT	–21.03	1.43	–19.60	57.10

[a] The ICA parameter was calculated using the UCSF Chimera 1.7 software according to the formula: (area of the host + area of the guest – area of the complex)/2, where the area refers to solvent-excluded molecular surfaces.[46]

Bulk solvent effects of DMF and TCE were evaluated using the integral equation formalism of the polarized continuum model (IEF-PCM) utilizing the universal force field (UFF) radii built from the UFF force field. Solvent effects were evaluated in single-point calculations for the previously optimized supramolecular structures in gas phase. As shown in Figure 4, the solvent effect produces in all cases a destabilization of the supramolecular guest-nanotube complex in the range of 0.72–1.80 kcal/mol for TCE and of 0.86–2.74 kcal/mol for DMF. The supramolecular assembly containing the pyrene-based guest **4** varies the most upon inclusion of solvent effects due to the presence of highly polar amine hydrogen atoms. This result is in line with the binding constant increase experimentally recorded for **4**•(6,5)-SWNT moving from the more polar DMF to the less polar TCE (log K_a = 1.43 and 2.84, respectively). Theoretical calculations were also performed using the continuum SMD model and resulted in larger destabilizations with respect to gas phase, but now the TCE solvent showed the largest differences (e.g., 9.16 kcal/mol in the case of **4**·(6,5)-SWNT, see Figure S10). Nonetheless, solvent effects evaluated by means of continuum solvent models (PCM or SMD) are not adequate to completely reproduce the trends in the association constants recorded experimentally when comparing DMF and TCE results (Table 1). Discrete guest-solvent interactions are expected to be key for

the accurate prediction of relative binding constants in different solvents and they are taken into account in the molecular dynamics simulations next discussed.

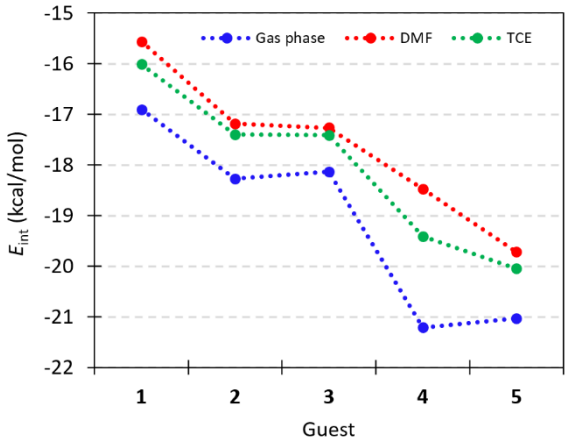

Figure 4. Effect of the solvent (DMF and TCE) on the interaction energy of the guest–nanotube assemblies using the polarizable continuum model PCM.

Adsorption free energies: To better understand the differences in association affinities when using DMF and TCE, we performed a set of molecular dynamics simulations in all-atom detail, using the CHARMM General Force Field (CGenFF).[47-50] In these simulations, we evaluated the association of the five guest molecules with the (6,5) single-wall carbon nanotubes used in the experiments and DFT calculations. The simplest model for probing this association consists of a single nanotube and a single guest molecule submerged in the solvent. However, note that this model is not the only plausible one; a model nanotube aggregate is also considered (see the Supporting Information). Examples of the isolated nanotube models are represented in Figure 5a,b. Using the adaptive biasing force method,[51-52] we calculated the free energy profile (potential of mean force) as a function of the distance between the axis of the nanotube and the center of mass of each guest molecule (ρ) (Figure 5c,d). The association is favorable for all guests in both solvents—significant free energy minima are apparent near $\rho \approx 7.15$ Å. In most cases, desolvation maxima[53] can be seen between 8.3 and 8.7 Å, followed by local minima between 9.7 and 10.0 Å. As observed in Figure S11, the global minima are associated with the guest molecules lying flat against the surface, while local minima near 9.7 and 10.0 Å correspond to larger angles between the guest molecules and the nanotube surfaces. Beyond 12 Å, the orientation becomes essentially randomly distributed, as indicated by the large standard deviations (Figure S11).

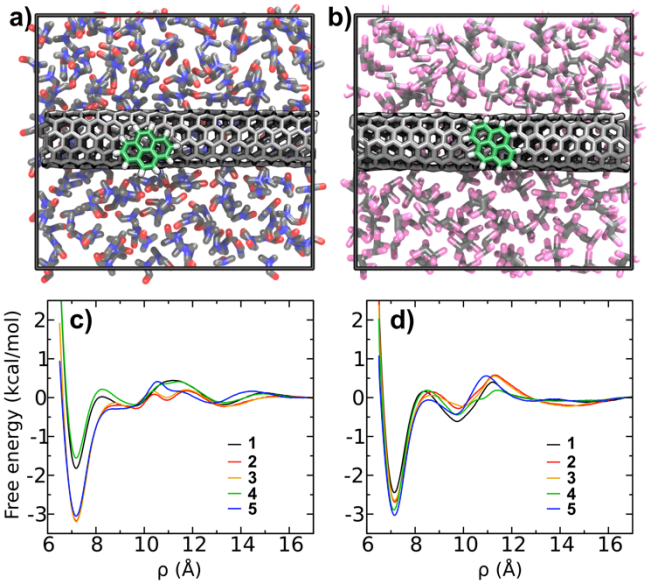

Figure 5. Molecular dynamics simulations of the association of pyrene derivatives **1–5** with an isolated carbon nanotube in DMF and TCE. (a,b) Exemplary snapshots of the molecular models used in the simulations. These snapshots include a guest molecule (pyrene, **1**) and DMF (a) or TCE (b) solvents. For clarity, solvent molecules above midplane of the nanotube and solvent H atoms are not shown. Guest C and H atoms are shown in green and white, respectively; other C atoms are gray. H, N, O, and Cl atoms are shown in white, blue, red, and magenta, respectively. Periodic boundary conditions are applied along all axes giving a nanotube that has effectively infinite length. (c,d) Free energy as function of the distance between the guest molecule and the axis of the nanotube in DMF (c) and TCE (d) solvents. The geometric contribution to the free energy, resulting from using a cylindrical radial coordinate, has been subtracted (see the Supporting Information) so that this function becomes flat for large separations between the guest and nanotube.

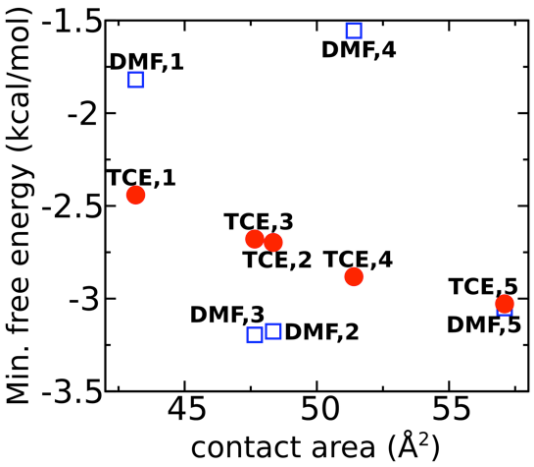

Figure 6. Correlation between the minimum free energy and the contact area in classical molecular dynamics simulations.

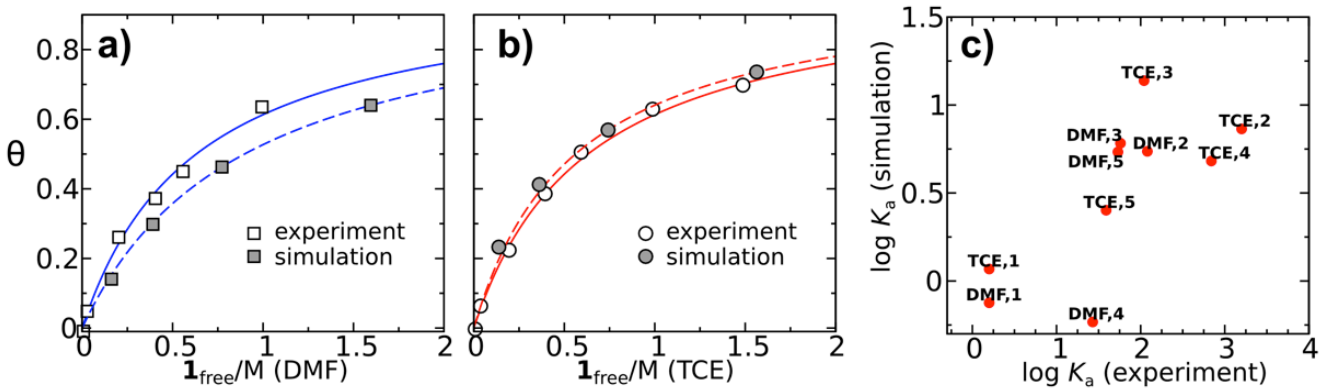

Figure 7. Titration molecular dynamics simulations. (a,b) Comparison of SWNT surface coverage of pyrene in DMF (a) and TCE (b) solvents as a function of the bulk pyrene concentration. Experimental data from Figure 1 is included for reference. (c) Comparison of the logarithm of the SWNT association constants (K_a) derived from experiment and simulation for the five guest molecules and two solvents.

In the non-polar solvent, TCE, the free-energy minima are highly correlated (R^2 = 0.97) with the contact area, which is consistent with the results of the DFT calculations (see Figure 3). On the other hand, as shown in Figure 6, the classical molecular dynamics calculations predict little correlation (R^2 = 0.08) between the contact area and adsorption free energy in DMF, a polar solvent. This lack of correlation in DMF is to be expected as polar interactions between the solvent and guest, such as those involving the amines of guest 4 or the carbonyl groups of guests **2** and **3**, are highly dependent on the chemical identities of the guests. In qualitative agreement with the experiments (see Table 1), the diamino pyrene derivative (**4**) has a much lower affinity for the nanotube in DMF than in TCE.

To more rigorously compare the titration experiments detailed in Figure 1 and the simulations, we performed equilibrium simulations that mimic them, using simulation systems similar to those in Figure 5a,b, but containing different numbers of guest molecules, allowing us to calculate the surface coverage as a function of the bulk guest concentration. As in the experiments, the association constants (K_a) were determined from fits of this function by the Langmuir adsorption isotherm. For pyrene (**1**), the results of these calculations are in very good agreement with titration experiments as shown in Figure 7a,b. For the other guests, the calculations predict lower affinities than those suggested by the experiments. The simulations give a range of log K_a from –0.3 to 1.1, while the experiments suggest a larger range from 0.2 to 3.2. It is likely that limitations of classical molecular force field contribute to this discrepancy, although other factors, such as aggregation of the nanotubes in the experiments may contribute as well (see Figures S12 and S13). Despite this disagreement, the relative values of K_a calculated in simulation were correlated with those derived from experiment, as shown in Figure 7c. We obtain a correlation coefficient for log K_a of R^2 = 0.41, which increases to R^2 = 0.73 when an outlier, guest 4 in DMF, is removed.

The titration simulations also demonstrate the molecular details underlying adsorption at high concentrations. As shown in Figure 8, the guest molecules differ in the structure of the adsorbed layers. For all guests, the first layer forms parallel to the SWNT surface. However, while guests **2**, **3**, and **5** form a well-defined second layer at a distance of 10.8 Å from the SWNT axis with the aromatic rings stacked parallel to those in the first layer, for guests **1** and **4** a second layer of molecules inserts between the molecules of the first at an oblique angle at a distance of 9.5 Å. Furthermore, the dione pyrene derivatives (**2** and **3**) form a prominent third stacked layer at distance of 14.6 Å. The other molecules show a small rise in density at 13.4 Å, suggesting less ordered overlayers.

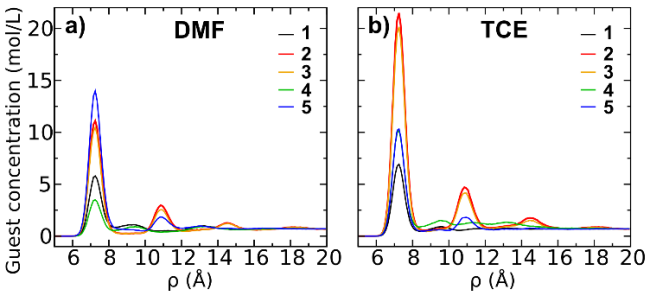

Figure 8. Multi-layer adsorption in simulations of adsorption to the SWNT. (a,b) Local guest concentration as a function of distance from the axis of the carbon nanotube in DMF (a) or TCE (b) solvent. The bulk concentration in these simulations was approximately 0.70 mol/L. For distances < 8 Å, the green curve (**4**) in panel b is nearly coincident with the blue curve (**5**) and therefore mostly hidden.

Conclusions

In conclusion, we report on a thorough quantitative characterization of the supramolecular recognition of soluble pyrene-based derivatives with insoluble (6,5)-SWNTs. Experimental binding constants measured by means of a thermogravimetric protocol demonstrate that solvophobic

interactions govern the self-assembly of small molecules with SWNTs. DFT calculations suggest that pyrene guests are able to interact through the aromatic skeleton by means of π–π forces with additional discrete contacts promoted by the chemical substitutions in the periphery of the pyrene core. Interestingly, the supramolecular stabilization is explained in terms of dispersion forces as suggested by the linear correlation between the intermolecular contact area and the interaction energy, whereas electronic charge-transfer effects are ruled out. Molecular dynamics with explicit solvent molecules allowed us to disentangle the molecular details underlying the adsorption process from low to high SWNT surface coverage.

Acknowledgements

This work was supported by the European Research Council (ERC-StG-MINT 307609), the Spanish Ministry of Economy and Competitiveness MINECO (CTQ2014-60541-P, CTQ2015-71154-P, CTQ2015-71936-REDT, and Unidad de Excelencia María de Maeztu MDM-2015-0538), the Generalitat Valenciana (PROMETEO/2016/135), and European FEDER funds (CTQ2015-71154-P). J.C. acknowledges the Ministerio de Educación, Cultura y Deporte (MECD) of Spain for a predoctoral FPU grant. This work was partially supported by the Kansas Bioscience Authority funds to the Institute of Computational Comparative Medicine (ICCM) at Kansas State University and to the Nanotechnology Innovation Center of Kansas State University (NICKS). Computing for this project was performed on the Beocat Research Cluster at Kansas State University, which is funded in part by NSF grants CNS-1006860, EPS-1006860, and EPS-0919443. This work used the Extreme Science and Engineering Discovery Environment (XSEDE), which is supported by National Science Foundation grant number ACI-1053575.

Keywords: carbon nanotubes • supramolecular chemistry • DFT • molecular dynamics

[1] R. J. Chen, Y. Zhang, D. Wang, H. Dai, *J. Am. Chem. Soc.* **2001**, *123*, 3838-3839.
[2] N. Nakashima, Y. Tomonari, H. Murakami, *Chem. Lett.* **2002**, *31*, 638-639.
[3] Y.-L. Zhao, J. F. Stoddart, *Acc. Chem. Res.* **2009**, *42*, 1161-1171.
[4] E. M. Pérez, N. Martín, *Chem. Soc. Rev.* **2015**, *44*, 6425-6433.
[5] G. Gavrel, B. Jousselme, A. Filoramo, S. Campidelli, in *Making and Exploiting Fullerenes, Graphene, and Carbon Nanotubes* (Eds.: M. Marcaccio, F. Paolucci), Springer Berlin Heidelberg, Berlin, Heidelberg, **2014**, pp. 95-126.
[6] N. Martín, J.-F. Nierengarten, *Supramolecular Chemistry of Fullerenes and Carbon Nanotubes*, Wiley-VCH, Weinheim, **2012**.
[7] D. M. Guldi, G. M. A. Rahman, F. Zerbetto, M. Prato, *Acc. Chem. Res.* **2005**, *38*, 871-878.
[8] D. M. Guldi, G. M. A. Rahman, N. Jux, N. Tagmatarchis, M. Prato, *Angew. Chem. Int. Ed.* **2004**, *43*, 5526-5530.
[9] C. Ehli, G. M. A. Rahman, N. Jux, D. Balbinot, D. M. Guldi, F. Paolucci, M. Marcaccio, D. Paolucci, M. Melle-Franco, F. Zerbetto, S. Campidelli, M. Prato, *J. Am. Chem. Soc.* **2006**, *128*, 11222-11231.
[10] D. R. Kauffman, A. Star, *Chem. Soc. Rev.* **2008**, *37*, 1197-1206.
[11] D. S. Hecht, R. J. A. Ramirez, M. Briman, E. Artukovic, K. S. Chichak, J. F. Stoddart, G. Grüner, *Nano Lett.* **2006**, *6*, 2031-2036.
[12] L. Hu, Y. L. Zhao, K. Ryu, C. Zhou, J. F. Stoddart, G. Grüner, *Adv. Mater.* **2008**, *20*, 939-946.
[13] F. Giacalone, N. Martin, *Adv. Mater.* **2010**, *22*, 4220-4248.
[14] X. Tu, M. Zheng, *Nano Res.* **2008**, *1*, 185-194.
[15] M. Zheng, A. Jagota, E. D. Semke, B. A. Diner, R. S. McLean, S. R. Lustig, R. E. Richardson, N. G. Tassi, *Nat. Mater.* **2003**, *2*, 338-342.
[16] L. Zhang, X. Tu, K. Welsher, X. Wang, M. Zheng, H. Dai, *J. Am. Chem. Soc.* **2009**, *131*, 2454-2455.
[17] X. Tu, S. Manohar, A. Jagota, M. Zheng, *Nature* **2009**, *460*, 250-253.
[18] H. Wang, Z. Bao, *Nano Today* **2015**, *10*, 737-758.
[19] N. Komatsu, F. Wang, *Materials* **2010**, *3*, 3818-3844.
[20] C. M. Homenick, G. Lawson, A. Adronov, *Polym. Rev.* **2007**, *47*, 265-290.
[21] D. Fong, W. J. Bodnaryk, N. A. Rice, S. Saem, J. M. Moran-Mirabal, A. Adronov, *Chem. Eur. J.* **2016**, *22*, 14560-14566.
[22] M. Imit, P. Imin, A. Adronov, *Polym. Chem.* **2016**, *7*, 5241-5248.
[23] X. Tu, S. Manohar, A. Jagota, M. Zheng, *Nature* **2009**, *460*, 250-253.
[24] S. Iliafar, J. Mittal, D. Vezenov, A. Jagota, *J. Am. Chem. Soc.* **2014**, *136*, 12947-12957.
[25] K. Tvrdy, R. M. Jain, R. Han, A. J. Hilmer, T. P. McNicholas, M. S. Strano, *ACS Nano* **2013**, *7*, 1779-1789.
[26] A. de Juan, A. López-Moreno, J. Calbo, E. Ortí, E. M. Peréz, *Chem. Sci.* **2015**, *6*, 7008-7014.
[27] D. Umadevi, S. Panigrahi, G. N. Sastry, *Acc. Chem. Res.* **2014**, *47*, 2574-2581.
[28] S. Grimme, A. Hansen, J. G. Brandenburg, C. Bannwarth, *Chem. Rev.* **2016**, *116*, 5105-5154.
[29] J. Calbo, E. Ortí, J. C. Sancho-García, J. Aragó, *J. Chem. Theory Comput.* **2015**, *11*, 932-939.
[30] J. Calbo, E. Ortí, J. C. Sancho-García, J. Aragó, in *Annual Reports in Computational Chemistry, Vol. 11* (Ed.: A. D. David), Elsevier, **2015**, pp. 37-102.
[31] S. Grimme, J. Antony, S. Ehrlich, H. Krieg, *J. Chem. Phys.* **2010**, *132*, 154104.
[32] S. Grimme, S. Ehrlich, L. Goerigk, *J. Comput. Chem.* **2011**, *32*, 1456-1465.
[33] A. Vila Verde, P. J. Beltramo, J. K. Maranas, *Langmuir* **2011**, *27*, 5918-5926.
[34] M. Hoefling, F. Iori, S. Corni, K.-E. Gottschalk, *Langmuir* **2010**, *26*, 8347-8351.
[35] R. Di Felice, S. Corni, *J. Phys. Chem. Lett.* **2011**, *2*, 1510-1519.
[36] G. Nawrocki, M. Cieplak, *J. Phys. Chem. C* **2014**, *118*, 12929-12943.
[37] Z. E. Hughes, L. B. Wright, T. R. Walsh, *Langmuir* **2013**, *29*, 13217-13229.
[38] G. Nawrocki, M. Cieplak, *Phys. Chem. Chem. Phys.* **2013**, *15*, 13628-13636.
[39] Z. E. Hughes, S. M. Tomasio, T. R. Walsh, *Nanoscale* **2014**, *6*, 5438-5448.
[40] Z. E. Hughes, T. R. Walsh, *J. Mater. Chem. B* **2015**, *3*, 3211-3221.
[41] R. Carr, J. Comer, M. D. Ginsberg, A. Aksimentiev, *J. Phys. Chem. Lett.* **2011**, *2*, 1804-1807.
[42] Z. W. Ulissi, J. Zhang, V. Sresht, D. Blankschtein, M. S. Strano, *Langmuir* **2015**, *31*, 628-636.
[43] J. Comer, R. Chen, H. Poblete, A. Vergara-Jaque, J. E. Riviere, *ACS Nano* **2015**, *9*, 11761-11774.
[44] A. López-Moreno, D. Clemente-Tejeda, J. Calbo, A. Naeimi, F. A. Bermejo, E. Ortí, E. M. Pérez, *Chem. Commun.* **2014**, *50*, 9372-9375.
[45] H. Wang, J. Mei, P. Liu, K. Schmidt, G. Jiménez-Osés, S. Osuna, L. Fang, C. J. Tassone, A. P. Zoombelt, A. N. Sokolov, K. N. Houk, M. F. Toney, Z. Bao, *ACS Nano* **2013**, *7*, 2659-2668.

[46] E. F. Pettersen, T. D. Goddard, C. C. Huang, G. S. Couch, D. M. Greenblatt, E. C. Meng, T. E. Ferrin, *J. Comput. Chem.* **2004**, *25*, 1605-1612.

[47] K. Vanommeslaeghe, E. Hatcher, C. Acharya, S. Kundu, S. Zhong, J. Shim, E. Darian, O. Guvench, P. Lopes, I. Vorobyov, A. D. Mackerell, *J. Comput. Chem.* **2010**, *31*, 671-690.

[48] W. Yu, X. He, K. Vanommeslaeghe, A. D. MacKerell, *J. Comput. Chem.* **2012**, *33*, 2451-2468.

[49] K. Vanommeslaeghe, A. D. MacKerell, *J. Chem. Inf. Model.* **2012**, *52*, 3144-3154.

[50] K. Vanommeslaeghe, E. P. Raman, A. D. MacKerell, *J. Chem. Inf. Model.* **2012**, *52*, 3155-3168.

[51] E. Darve, A. Pohorille, *J. Chem. Phys.* **2001**, *115*, 9169-9183.

[52] J. Comer, J. C. Gumbart, J. Hénin, T. Lelièvre, A. Pohorille, C. Chipot, *J. Phys. Chem. B* **2015**, *119*, 1129-1151.

[53] J. Chen, C. L. Brooks, H. A. Scheraga, *J. Phys. Chem. B* **2008**, *112*, 242-249.

Layout 2:

FULL PAPER

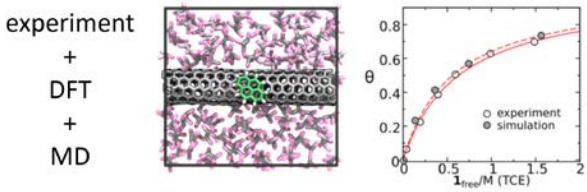

We present a quantitative multidisciplinary approach to understand noncovalent interactions between small molecules and SWNTs, including experiment, DFT and MD calculations.

J. Calbo,[a] A. López-Moreno,[b] A. de Juan,[b] J. Comer,[c,] E. Ortí,[a,*] E. M. Pérez[b,*]*

Page No. – Page No.

Understanding Noncovalent Interactions of Small Molecules with Carbon Nanotubes